Available online at www.sciencedirect.com
ScienceDirect
Journal of the European Ceramic Society 29 (2009) 2199–2209
www.elsevier.com/locate/jeurceramsoc

The system Clinker–MgO–$CaZrO_3$ and its application to the corrosion behavior of $CaZrO_3$/MgO refractory matrix by clinker

S. Serena, M.A. Sainz, A. Caballero *

Instituto de Cerámica y Vidrio (CSIC), C/Kelsen 5, Cantoblanco, 28049 Madrid, Spain

Received 24 September 2008; received in revised form 14 January 2009; accepted 14 January 2009
Available online 23 February 2009

Abstract

Phase relations in the clinker-rich region and the limits between the different stability fields of the isothermal section Clinker (CK)–MgO–$CaZrO_3$ at 1500 °C were experimentally established. The corrosion behavior by clinker of Portland cement of a $CaZrO_3$-rich/MgO refractory matrix obtained from both natural and synthetic raw materials were also studied. The attack mechanism to $CaZrO_3$-rich substrates was discussed in terms of microstructural features of the refractory matrix and the information supplied by the isothermal section Clinker–MgO–$CaZrO_3$ at 1500 °C.

Keywords: Clinker; Corrosion; Refractories; Clinker–MgO–$CaZrO_3$ system; Chrome-free refractories; MgO–$CaZrO_3$ refractory matrix

1. Introduction

Magnesia–chromite bricks have been standard lining material for the hot kiln zones since ~1940. Their properties, e.g. thermal conductivity, resistance to thermal shock and thermal expansion, are mainly determined by the use of refractory grade chrome ores.[1]

However, the presence of alkalis in an oxidizing atmosphere can cause the chrome-ore of magnesia–chromite bricks to degenerate producing the formation of toxic hexavalent chromates.[2,3] Recently, an increase in environmental concerns has put pressure on manufacture companies to strive for zero-emission status or to achieve the environmental isocertification.

MgO and $CaZrO_3$ are compatible phases and do not form a liquid phase up to temperatures higher than 2060 °C.[4,5] These materials have been suggested as chrome-free refractories for cement kilns to replace not only magnesia–chromite, but also the magnesia-oversaturated spinel now used as an alternative. MgO-spinel bricks are highly resistant to thermal shock, non-sensitive against reducing/oxidizing conditions, but are vulnerable to thermal overload. Spinel also forms low-melting phases with the result of premature wear. The analysis of MgO/$CaZrO_3$ as refractory materials in rotary cement kilns carried out by Kozuka et al.[6,7] points out to a good behavior on service of this material. More recently, the behavior against corrosion by clinker of MgO-rich/$CaZrO_3$ matrices at high temperatures was established by Serena et al.[8] In this study, the authors put in evidence that the corrosion process causes the formation of an MgO sintered layer on the substrates that stopped the progress of the attack. Moreover, after the corrosion test, a clinker layer remained adhered on the substrate surfaces that could contribute to prevent the corrosion of the refractory brick under work conditions. These results underline the good corrosion behavior of the MgO–$CaZrO_3$ materials, and support their use as a matrix in magnesia chrome-free bricks for the burning zone of rotary cement kilns.

Recently Rodríguez-Galicia et al.,[9] studied the chemical reactions involved in the corrosion of magnesia–calcium zirconate–calcium silicate materials up to 1600 °C using a hot-stage microscopy and SEM-EDS studies. They found that the corrosion occurs by a diffusion mechanism of the clinker liquid phase through grain boundary and open pores. These authors also claimed that materials containing 31 wt.% and 35 wt.% $CaZrO_3$ react with the clinker liquid phase and form a zirconium-containing silicate liquid boundary layer. The presence of Zr^{4+} in this liquid phase increases its viscosity and consequently the corrosion resistance of these materials. Also they made a comparative study of an aluminum magnesium spinel sample and

* Corresponding author.
E-mail address: acaballero@icv.csic.es (A. Caballero).

0955-2219/$ – see front matter © 2009 Elsevier Ltd. All rights reserved.
doi:10.1016/j.jeurceramsoc.2009.01.015

found that the spinel was markedly dissolved, up to 30 wt.%, which explains the limited corrosion behavior of spinel magnesia refractories currently used in the clinkering zone of the rotary cement kilns.

Finally, Park[10] has carried out computational and experimental studies on the formation of $CaZrO_3$ at the slag–MgO interface. They conclude that a ZrO_2 addition produces $CaZrO_3$ formation at the interface, which increases the refractory life but limits the refining ability of the slag.

The promising results observed in MgO-rich/$CaZrO_3$ matrices and the cited results by Rodríguez-Galicia et al.,[9] moved the present authors to inquire into the effect of $CaZrO_3$ content on the response of the matrix to the attack by clinker. As pointed out in the previous work[8] the reaction process between MgO/$CaZrO_3$ refractory matrices and clinker can be studied and discussed in terms of the MgO–CaO–ZrO_2–SiO_2 system, and, more specifically, on the quaternary system MgO–$CaZrO_3$–Ca_2SiO_4(C_2S)–Ca_3SiO_5(C_3S). However, to advance in the knowledge of the real system the isothermal section at 1500 °C of the clinker-rich region of the Clinker–MgO–$CaZrO_3$ system has been experimentally established. After that, the behavior against corrosion of a matrix constituted by 80% $CaZrO_3$ (wt.%) and 20% MgO (wt.%) was analyzed.

2. Experimental procedure

The starting materials were high-purity powders of m-ZrO_2 (TZ-0, 99.9 wt.%, Tosoh Corp., Tokyo, Japan) with an average size, d_{50} <0.87 μm; high-purity dolomite ($MgCa(CO_3)_2$; Micro15, 99.9 wt.%, Prodomasa, Málaga, Spain) with d_{50} < 4.87 μm; $CaZrO_3$ (>97 wt.%, ALFA Aesam Jonhson Matthey Company, Karlsruhe, Germany) with a bimodal size distribution centered in d_{50} = 0.27 μm and d_{50} = 1.3 μm; and MgO (>97 wt.%, MERCK, Darmstadt, Germany) with a d_{50} <38.8 μm. The clinker (CK) used was a Portland cement with the following chemical (wt.%) and mineralogical characteristics: Al_2O_3 5.70; MgO 1.50; CaO 66.06; SiO_2 21.25; Fe_2O_3 3.90; SO_4^{2-} 0.85; weight loss at 1000 °C was 0.28%. At 1500 °C the clinker shows Ca_3SiO_5 (C_3S) and liquid as stables phases.

Calcium zirconate, magnesium oxide and clinker were used as raw materials for establishing phase relations in the Clinker–MgO–$CaZrO_3$ isothermal section at 1500 °C of the MgO–$CaZrO_3$–$Ca_4Al_2Fe_2O_{10}$–Ca_3SiO_5 system. The mixed powders of each composition (Table 1) were homogenized in acetone and dried at 60 °C. The powders were hand pressed in a Pt crucible and fired in a bottom loading elevator furnace at 1500 °C. The heating rate was 5 °C/min up to 1500 °C and temperature was held there for 12 h. After the thermal treatment, the samples were air-quenched. Phase identification was based on X-ray diffraction (Siemens D-5000) and scanning electron microscopy with energy-dispersive X-ray analyzer (SEM-EDS, Zeiss DMS 950, Germany).

Several samples with final composition, 80 wt.% $CaZrO_3$ and 20 wt.% MgO were prepared to be used as substrates during the corrosion test. Substrates (20M–80CZ/D), (20M–80CZ/C) were obtained from mixtures of m-ZrO_2 and dolomite $CaMg(CO_3)_2$ and mixtures of commercial $CaZrO_3$ and MgO respectively. The processing route proposed was the following: the mixed powders of both compositions were first homogenized with isopropyl alcohol in an attrition miller for 2 h, dried at 60 °C followed by 60 μm sieving and isostatic pressing at 200 MPa to form a green compact. Dense substrates (>98 wt.% of theoretical density) were obtained by heating of the samples at 1600 °C for 2 h. Dense cylinders were cut to obtain discs 10 mm in diameter and 2 mm in height.

Table 1
Compositions formulated in the Clinker–MgO–$CaZrO_3$ system.

Name	Composition (wt.%)			Phase assemblage
	Clinker	MgO	$CaZrO_3$	
CK70M1	70	15	15	Liquid, Ca_3SiO_5, $CaZrO_3$, MgO
CK80M1	80	10	10	Liquid, Ca_3SiO_5, $CaZrO_3$, MgO
CK85M1	85	1	14	Liquid, Ca_3SiO_5, $CaZrO_3$
CK85M2	85	5	10	Liquid, Ca_3SiO_5, $CaZrO_3$, MgO
CK85M3	85	7.5	7.5	Liquid, Ca_3SiO_5, $CaZrO_3$, MgO
CK85M4	85	10	5	Liquid, Ca_3SiO_5, $CaZrO_3$, MgO
CK85M5	85	14	1	Liquid, Ca_3SiO_5, MgO
CK90M1	90	2	8	Liquid, Ca_3SiO_5, $CaZrO_3$
CK90M2	90	3.5	6.5	Liquid, Ca_3SiO_5, $CaZrO_3$, MgO
CK90M3	90	5	5	Liquid, Ca_3SiO_5, $CaZrO_3$, MgO
CK90M4	90	8	2	Liquid, Ca_3SiO_5, MgO
CK95M1	94	1	5	Liquid, Ca_3SiO_5, $CaZrO_3$
CK95M2	94	3	3	Liquid, Ca_3SiO_5, $CaZrO_3$, MgO
CK95M3	94	5	1	Liquid, Ca_3SiO_5, MgO
CK98M4	98	1	1	Liquid, Ca_3SiO_5

Hand-pressed pieces of 1.5 mm × 1.5 mm and 2 mm of clinker of cement were deposited on both substrate surfaces. The couples clinker–substrate were thermally treated at 5 °C/min up to 1500 °C/and maintained for 1 min or 3 h, then cooled at 10 °C/min. Microstructural analysis and phase identification were done by optical microscopy and Scanning Electron Microscopy (Zeiss DMS 950, Germany) with Energy-Dispersive X-ray Analyzer (SEM-EDS).

3. Results and discussion

3.1. Isoplethal section Clinker (CK)–MgO–$CaZrO_3$ at 1500 °C

At 1500 °C the clinker is constituted by Ca_3SiO_5 (C_3S) and a liquid phase. The liquid phase contains not only calcium and silicon oxides but also other main impurities, such as iron oxide, aluminum oxide and magnesium oxide (Table 2). The primary volume of crystallization of C_3S in the CaO–SiO_2–MgO–Al_2O_3–Fe_2O_3 system is very useful for a proper understanding of the corrosion behavior of refractory matrices by clinker. Fig. 1 shows the primary volume of C_3S in the CaO–Ca_2SiO_4 (C_2S)–$Ca_4Al_2Fe_2O_{10}$ (C_4AF)–Al_2O_3 subsystem constructed from bibliographic information.[11–17] From this figure it can be deduced that C_4AF phase is compatible with C_3S and C_2S and that Al_2O_3 and Fe_2O_3 are the main impurities in the clinker, since drastically decrease the

Table 2
Composition of solid phases and liquids at 1500 °C/12 h determined by EDS. (n.d., not determined).

Sample	Phase	Oxide (wt.%)						
		MgO	Al_2O_3	SiO_2	CaO	Fe_2O_3	ZrO_2	TiO_2
Clinker	Liquid	2.8	23.7	3.	50.1	19.5	–	n.d.
	Ca_3SiO_5							
CK90M1	Liquid	3.4	15.8	4.8	51.6	16.5	6.3	1.6
	$CaZrO_3$	–	–	–	38.3	–	61.7	–
	Ca_3SiO_5	2.0	0.6	24.5	72.4	0.5	–	–
CK90M3	Liquid	2.6	14.9	4.5	49.4	15.9	11.2	1.5
	MgO	97.1	–	–	1.7	1.2	–	–
	$CaZrO_3$	–	–	–	38.0	–	62.0	–
	Ca_3SiO_5	1.8	1.0	25.5	71.4	0.3	–	–
CK90M4	Liquid	2.6	16.2	6.8	49.5	14.7	8.8	1.4
	MgO	97.2	–	–	1.5	1.3	–	–
	Ca_3SiO_5	1.9	1.0	23.4	72.7	1.0	–	–

temperature of first liquid formation in the system. Consequently C_4AF is the first solid phase dissolved in the liquid phase and is not present in the clinker at temperatures higher than 1350 °C. Fig. 2a shows the primary crystallization volume of C_3S and C_2S in the MgO–CaO–C_4AF–C_2S subsystem.[18,19] Fig. 2b schematically shows the location of clinker composition in the C_4AF–MgO–C_3S/C_2S pseudoternary system and the phase assemblages at temperatures higher than 1350 °C. The C_3S/C_2S corner corresponds with clinker ratio and L is liquid. From the quaternary system, Fig. 2a, it can be deduced the limited effect of MgO on the first—liquid formation temperature of clinker. Finally from both diagrams it can be deduced that C_4AF, C_2S, C_3S, and MgO phases are compatible in the solid state.

Since calcium zirconate (CZ) is compatible in the solid state with C_3S, C_2S and C_4AF, a schematic representation (Fig. 3a) showing the primary crystallization volumes of C_3S and C_2S in the $CaZrO_3$ (CZ)–C_2S–C_3S–C_4AF quaternary subsystem has been made.[8,20–22] Fig. 3b shows the pseudoternary section C_3S/C_2S–$CaZrO_3$–C_4AF at temperatures higher than 1350 °C. In this figure, the C_3S/C_2S corner corresponds with clinker ratio, and MgO has been not considered in this representation due to the fact that clinkers usually present small amounts of this phase, and its effect on the temperature of clinker melting is almost negligible. Given that the temperatures of the invariant points are extremely high in the C_3S–C_2S–CZ ternary subsystem, C_4AF is the phase which drastically reduces the temperature of first liquid formation in the CZ–C_2S–C_3S–C_4AF quaternary subsystem, and consequently is the first solid phase dissolved in the liquid phase at high temperature.

From all previously deductions a schematic representation of the C_3S/C_2S–MgO–CZ–C_4AF system has been done (Fig. 4). From this figure and taking into account that C_4AF is dissolved in the liquid phase at temperatures higher than 1350 °C and

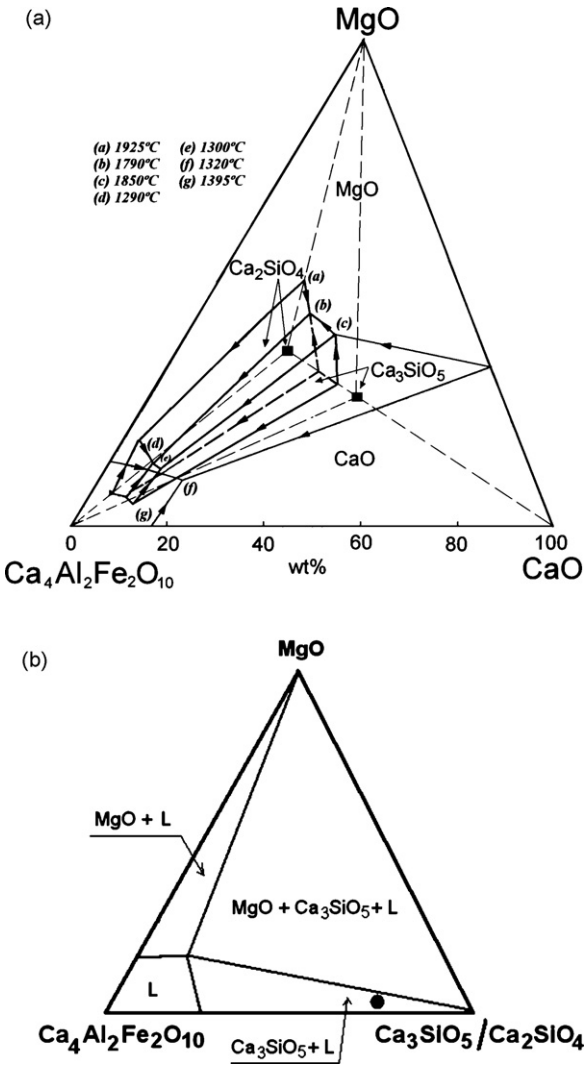

Fig. 2. (a) Schematic representation showing primary volume of crystallization of Ca_3SiO_5 in the subsystem MgO–$Ca_4Al_2Fe_2O_{10}$–CaO–Ca_2SiO_4. (b) Schematic representation of an isothermal section at temperatures between 1395 °C and 1790 °C of the isoplethal section Clinker–MgO–$Ca_4Al_2Fe_2O_{10}$. The point (•) represents clinker composition.

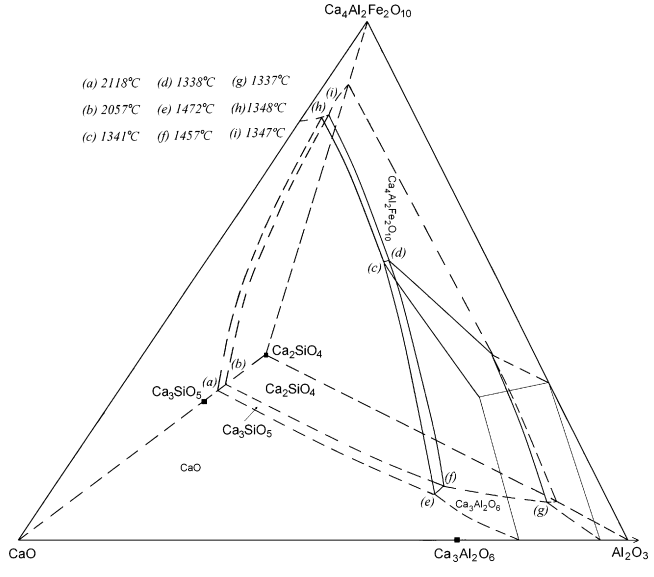

Fig. 1. Schematic representation showing primary volume of crystallization of Ca_3SiO_5 in the subsystem CaO–Ca_2SiO_4–$Ca_{12}Al_{14}O_{33}$–$Ca_4Al_2Fe_2O_{10}$.

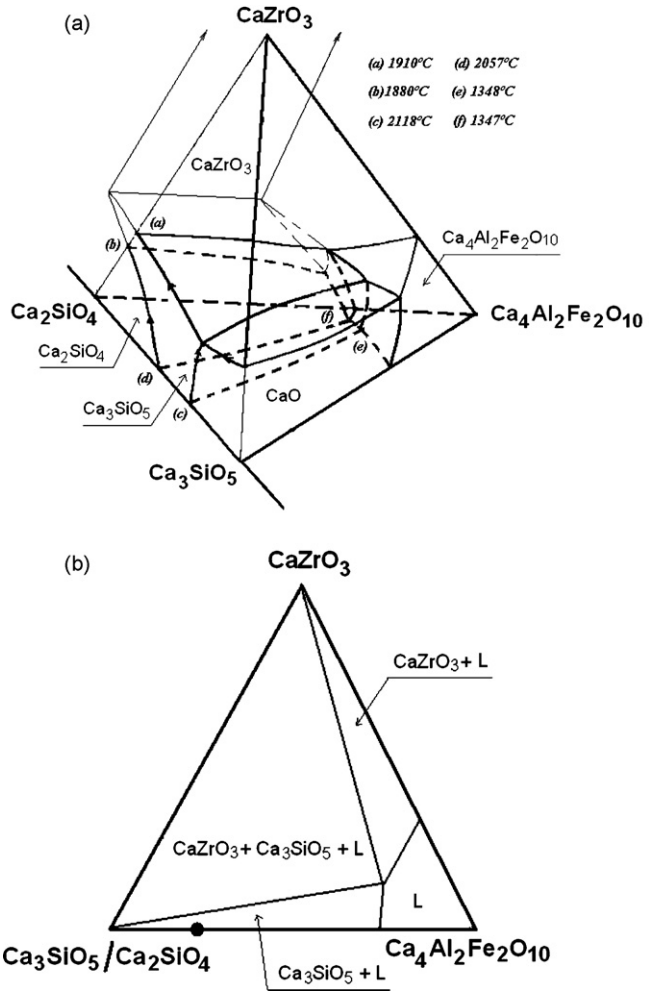

Fig. 3. (a) Schematic representation showing primary volume of Ca_3SiO_5 in the subsystem $CaZrO_3$–$Ca_4Al_2Fe_2O_{10}$–CaO–Ca_2SiO_4. (b) Schematic representation of an isothermal section at temperatures between 1350 °C and 2000 °C of the isoplethal section Clinker–MgO–$Ca_4Al_2Fe_2O_{10}$. The point (•) represents clinker composition.

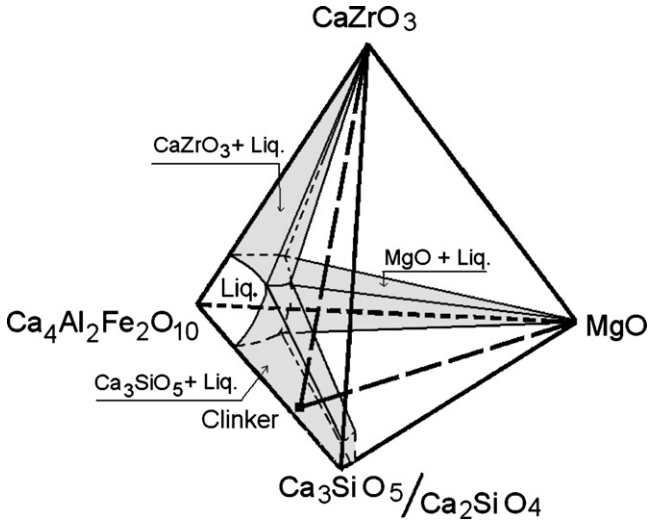

Fig. 4. Schematic representation showing primary volumes of crystallization of compatible phases and the liquid volume at 1500 °C in the subsystem MgO–$CaZrO_3$–Ca_3SiO_5–$Ca_4Al_2Fe_2O_{10}$. The isoplethal section Clinker–$CaZrO_3$–MgO also is shown.

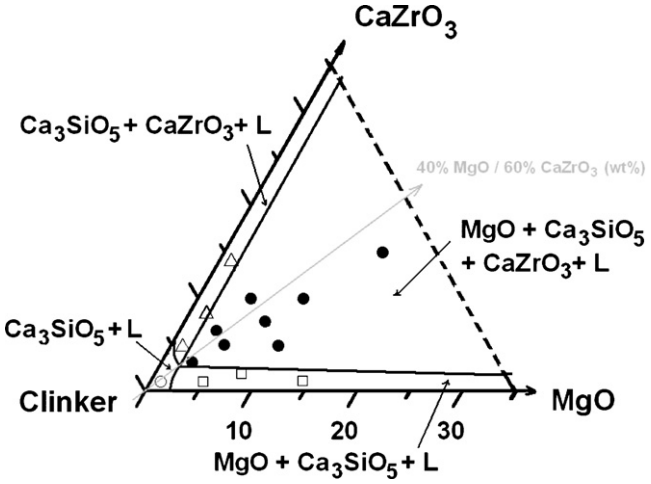

Fig. 5. The Clinker–MgO–$CaZrO_3$ system at 1500 °C. The figure shows the compatibility fields intersected by the section. The fine line defines the $CaZrO_3$/MgO ratio (1.5 wt.%) which produces the precipitation of calcium zirconate (>1.5 wt.%) or magnesia (<1.5 wt.%), as secondary crystalline phase, in the clinker.

that clinker is constituted at 1500 °C by C_3S and Liquid,[23] the isoplethal section CK–MgO–$CaZrO_3$ is a clinker-specific pseudo-ternary section constituted by C_3S, MgO, $CaZrO_3$ and liquid phase, where the composition of the liquid will change as a function of Clinker–MgO–$CaZrO_3$ starting composition.

Phase relations in the clinker-rich region of this section were experimentally established at 1500 °C for the compositions shown in Table 1. This table also shows the phase assemblages for each composition. XRD was decisive for determining the presence of crystalline phases while SEM observation was essential to establish the presence of a liquid phase in the samples.

The solid solution of magnesia (MgO), alumina (Al_2O_3) and iron oxide (Fe_2O_3) in tricalcium silicate (Ca_3SiO_5); calcium oxide (CaO) and iron oxide (Fe_2O_3) in magnesium oxide and the composition of the liquid phase in selected samples located in the (C_3S + Liq + $CaZrO_3$), (C_3S + Liq + MgO) and (C_3S + Liq + $CaZrO_3$ + MgO) fields were determined by SEM-EDS at 1500 °C (Table 2). No solid solution of CaO, MgO and/or ZrO_2 was found in calcium zirconate ($CaZrO_3$). No binary or ternary compounds were found, since magnesium oxide, calcium zirconate and tricalcium silicates are compatible phases as previously established.

The isothermal section of the clinker-rich CK–MgO–$CaZrO_3$ at 1500 °C deduced from these experimental results is depicted in Fig. 5. The section shows a large four-phase area (C_3S–MgO–$CaZrO_3$–Liq), two narrow three-phase regions, ($CaZrO_3$–C_3S–Liq), (C_3S–MgO–Liq) and one two-phase area (C_3S + Liq). The small size of two-phase and three-phase regions and the big size of the four-phase area put in evidence that clinker treated at 1500 °C (C_3S + Liq), shows a very limited solubility for MgO and $CaZrO_3$. Nevertheless, the MgO dissolved in the liquid phase is clearly less than $CaZrO_3$, as can be deduced from the ZrO_2 content in the liquid phase (Table 2). No field of liquid phase region as lonely phase was found in the isothermal section.

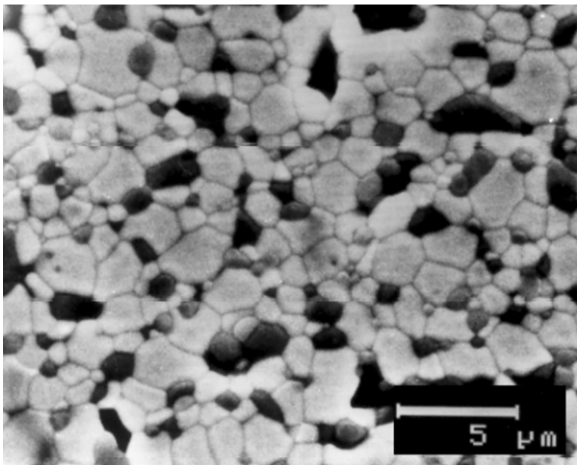

Fig. 6. SEM micrographs showing the microstructure of the 20M–80CZ/D sample treated at 1600 °C/2 h. Bright grains are $CaZrO_3$ and dark grains are MgO.

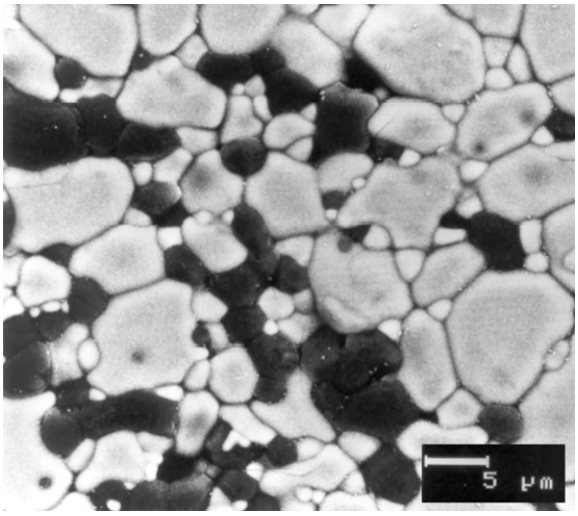

Fig. 7. SEM micrographs showing the microstructure of the 20M–80CZ/C sample treated at 1600 °C/2 h. Bright grains are $CaZrO_3$, dark grains are MgO and smallest and brightest grains are ZrO_2.

The thin line of Fig. 5 defines the $CaZrO_3$/MgO ratio (1.50 wt.% ± 0.15), which produces the precipitation of $CaZrO_3$ or MgO as secondary crystalline phase in the clinker (C_3S is always the primary crystalline phase). An important practical implication can be deduced from the results obtained; the formation of the MgO or $CaZrO_3$ layer at the interface of the clinker–substrate will depend on the $CaZrO_3$/MgO ratio, since ratios higher or lower than 1.5 wt.% will give $CaZrO_3$ or MgO layer at the interface.

An error around 10 wt.% has been assessed considering that the point which defines the ratio is closer to the clinker corner and consequently small variations in the limits of the field will produce big deviations on the projection of this point on the calcium zirconate/magnesia side of the system.

Finally, remark that the section studied (1500 °C) is specific to the clinker used, but big differences for others clinkers are not expected considering the relatively high similitude of the chemical and mineralogical compositions of the commercial clinkers.

3.2. Clinker–substrate corrosion test

3.2.1. Microstructural feature of substrates

The microstructure of the substrates, 20M–80CZ/D and 20M–80CZ/C, observed by SEM is shown in Figs. 6 and 7. The substrates can be described as a matrix of $CaZrO_3$ (bright phase) and MgO grains (dark phase) generally located at matrix grain boundaries and triple points. Both substrates presented about 98% theoretical density and mainly intergranular porosity. In the substrate 20M–80CZ/D (Fig. 6), $CaZrO_3$ grains with a size between 0.5 and 4 μm and MgO grains <2 μm were observed. In 20M–80CZ/C sample, the size of the $CaZrO_3$ grains varied between 5 and 15 μm while MgO grains usually varied from 2 to 5 μm. Occasionally MgO agglomerates were also found with a size between 10 and 15 μm (Fig. 7). In this substrate is also remarkable the presence of bright grains, <1 μm, corresponding to zirconia, resulting of an excess of ZrO_2 in the formulation of the commercial $CaZrO_3$.

The differences observed between both substrates are related not only with the composition of the raw materials and the microstructural features development, but also with the reaction process. In the case of 20M–80CZ/C composition, the sub-

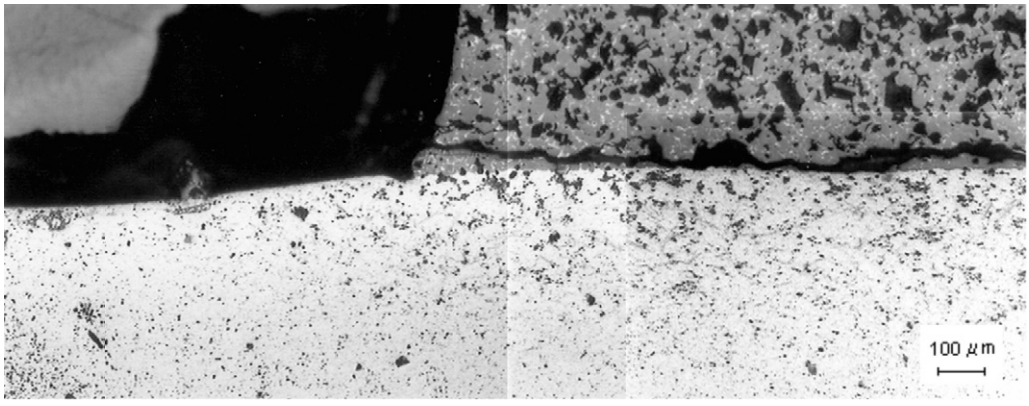

Fig. 8. Polished cross-sections observed by reflected light optical microscopy of the sample Clinker–20M–80CZ/D substrate treated at 1500 °C/1 min.

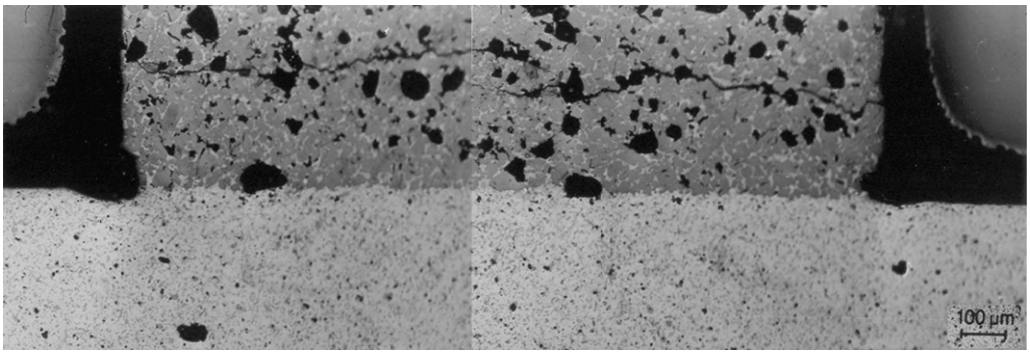

Fig. 9. Polished cross-sections observed by reflected light optical microscopy of the sample Clinker–20M–80CZ/C substrate treated at 1500 °C/1 min.

strate was obtained by a sintering process on samples previously synthesized (rich-ZrO_2 calcium zirconate), while in the case of the 20M–80CZ/D composition, the substrate was obtained by a reaction-sintering process which produces a finer and more homogeneus microstructural development.[24,25]

3.2.2. Corrosion test 1500 °C/1 min

Figs. 8 and 9 show the polished cross-sections observed by optical microscopy of both substrates reacted with clinker at 1500 °C/1 min. Note that the pictures are actually compositions of two photographs showing all the relevant features of the cross-section. In both cases the bulk clinker appears separated of the substrates by a breaking line. In the 20M–80CZ/C sample there is a homogeneous layer (200–300 μm) of clinker adhered to the substrate under the breaking line, while in the 20M–80CZ/D substrate the breaking line is closer or in the interphase. In this case, the thickness of the adhered layer was clearly inhomogeneous, reaching 30 μm, in some places.

Figs. 10 and 11 show the polished cross-sections observed by SEM whereby the reaction between clinker and substrates were more easily observed. As a consequence of the reaction between clinker and substrate, different interaction areas can be recognized (Figs. 10a and 11a). Zone 1 corresponds to the original clinker; zone 2 is defined by the clinker layer adhered to the substrate surface and zone 3 is the reaction area, that occurs at the interphase. SEM-EDS technique was used to determine the composition of the liquid and solid phases in the defined zones (Table 3).

In both samples, EDS microanalysis performed in the zone 1, far enough from the interaction area, allowed us to establish that C_3S and a liquid phase were the only stable phases. In the zone 2 the layer was also constituted by C_3S and liquid, although non-dissolved, isolated round grains of $CaZrO_3$ and MgO were detected, especially in the 20M–80CZ/C sample because of the larger grain size of this substrate. The composition of the liquid phase measured in this zone is also shown in Table 3. The dissolution of $CaZrO_3$ from the substrate and C_3S from the clinker produces an increase in ZrO_2, CaO and SiO_2 in the liquid phase, but not significant changes in the MgO content of this phase. This dissolution process also makes the Al_2O_3 and Fe_2O_3 content in the liquid in the zone 2 to decrease with respect to the corresponding liquid in zone 1. The higher ZrO_2 content observed in

Table 3
Average composition of the liquid phase, in the clinker near the interaction (zone 2 in Figs. 10 and 11), determined by EDS, after the thermal treatment at 1500 °C/1 min.

Substrate	Zone	Composition of the liquid phase (wt.%)					
		CaO	Al_2O_3	Fe_2O_3	SiO_2	MgO	ZrO_2
20M–80CZ/D	Zone 2	62.5	6.1	7.5	17.3	2.1	4.4
20M–80CZ/C	Zone 2	60.4	5.2	6.8	17.1	0.9	9.6

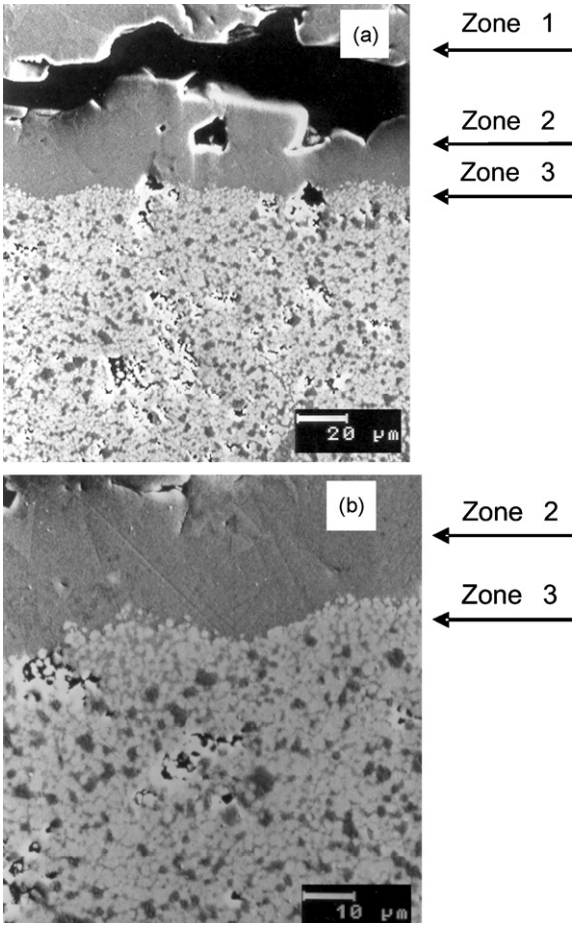

Fig. 10. (a) General view by SEM of the different interaction areas in the sample Clinker–20M–80CZ/D treated at 1500 °C/1 min. (b) SEM micrographs showing the interface and the interaction between clinker and substrate at higher magnification.

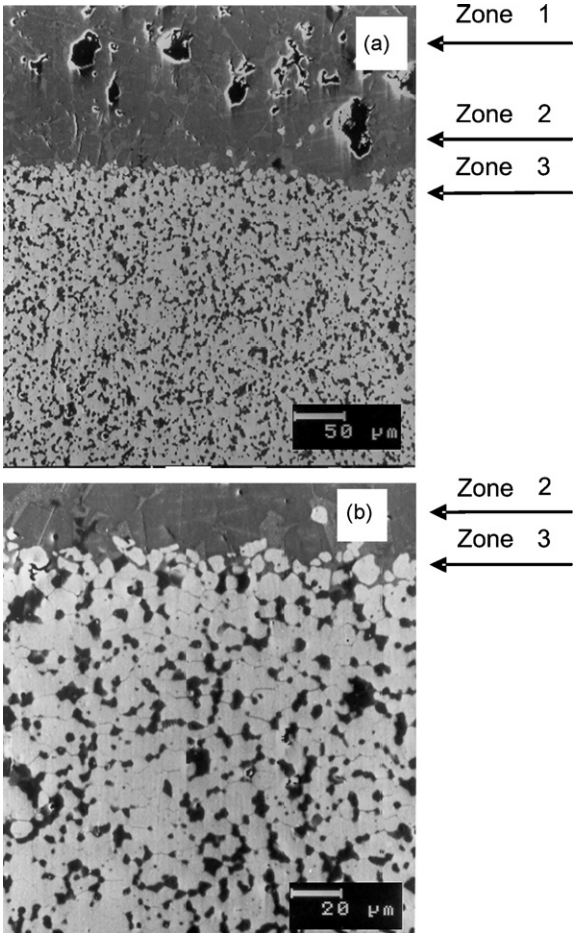

Fig. 11. (a) General view by SEM of the different interaction areas in the sample Clinker–20M–80CZ/C treated at 1500 °C/1 min. (b) SEM micrographs showing the interface and the interaction between clinker and substrate at higher magnification.

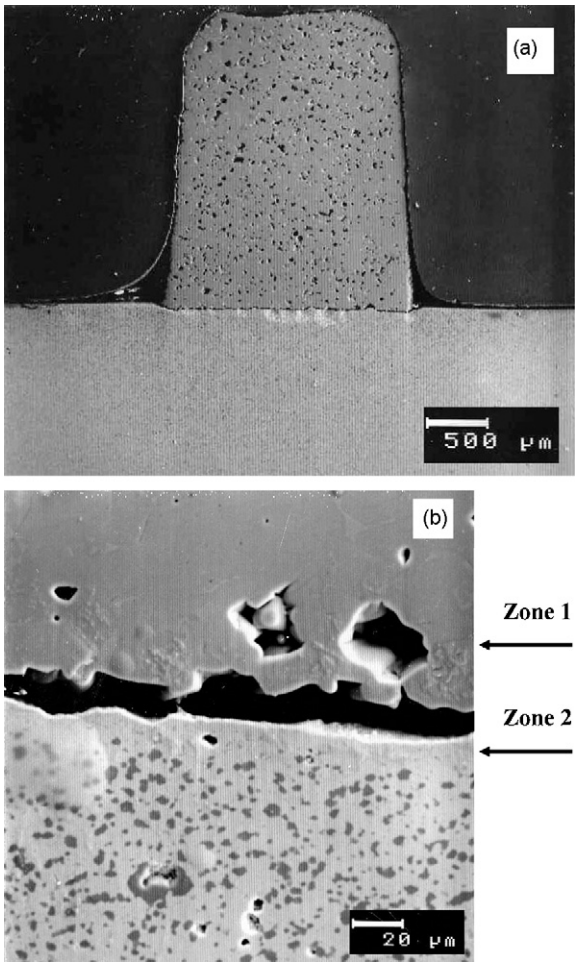

Fig. 12. (a) General view of the sample Clinker–20M–80CZ/D treated at 1500 °C/3 h. (b) SEM micrographs showing the interface and the interaction areas between clinker and substrate at higher magnification.

the liquid phase in 20M–80CZ/C sample is due to the excess of ZrO_2 in the original substrate.

The thickness of the reaction area, zone 3 in Figs. 10 and 11, was around 10 μm in the 20M–80CZ/D sample and hardly detectable in 20M–80CZ/C substrate. The reaction area in the sample 20M–80CZ/D was characterized by the absence of MgO grains and the presence of rounded shape $CaZrO_3$ grains evolved in the liquid phase (Fig. 10b). No other phases were observed in this area and the small amount of the liquid phase made it impossible to obtain reliable EDS-values for this phase. The reaction area in the second sample (Fig. 11b) shows a weak interaction between the sample and the clinker and only two o three layers of grains showed corrosion features. In both samples, under the interaction zone, the substrates maintain their initial microstructure, and only a small quantity of liquid phase, diffused through grain boundaries and pores, was observed.

3.2.3. Corrosion test 1500 °C/3 h

Figs. 12 and 13 show SEM micrographs of the polished cross-section of clinker–substrates samples after firing at 1500 °C for 3 h. It is important to remark that, in both samples, the clinker penetrated about 50 μm into the substrates (Figs. 12a and 13a),

Table 4
Average composition of the liquid phase near the interaction zone (zone 1 in Figs. 12 and 13) and interaction zone inside the substrates (zone 2 in Figs. 12 and 13), determined by EDS after the thermal treatment at 1500 °C/3 h.

Substrate	Zone	Composition of the liquid phase (oxide (wt.%))					
		CaO	Al_2O_3	Fe_2O_3	SiO_2	MgO	ZrO_2
20M–80CZ/D	Zone 1	50.1	24.1	18.2	3.9	2.8	0.8
	Zone 2	49.2	22.9	20.4	3.9	2.6	0.9
20M–80CZ/C	Zone 1	53.6	15.0	21.6	4.4	2.1	3.4
	Zone 2	48.6	11.3	18.4	4.4	5.4	11.9

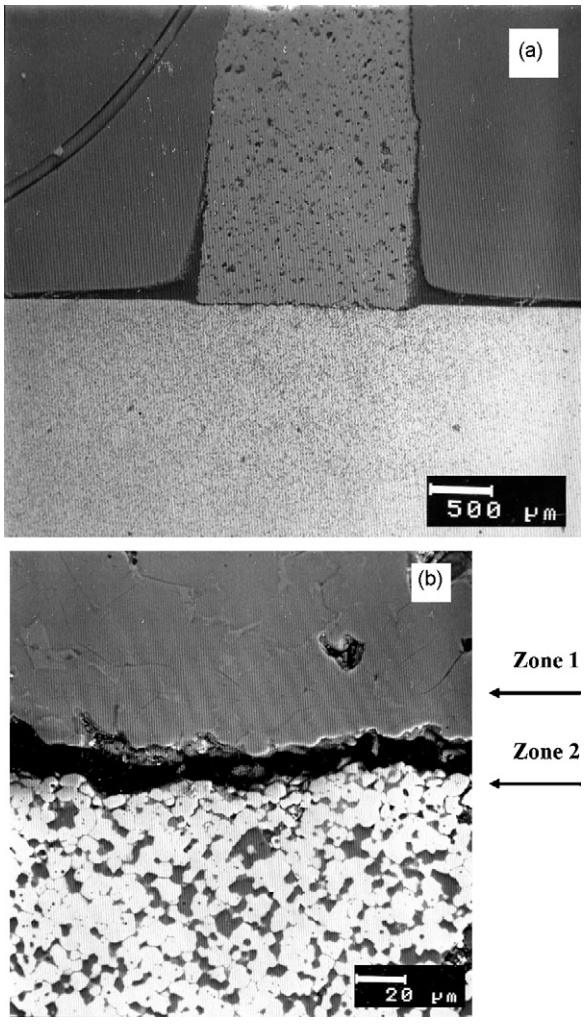

Fig. 13. (a) General view of the sample Clinker–20M–80CZ/C treated at 1500 °C/3 h. (b) SEM micrographs showing the interface and the interaction areas between clinker and substrate at higher magnification.

but appears completely separated from them. No longitudinal or transversal cracks at the interfaces, or clinker adhered on the surface could be observed at higher magnifications (Figs. 12b and 13b). In these experiments only two differential areas can be recognized. The first area (zone 1) corresponds to the clinker and the second one (zone 2) is the reaction zone that occurs in the interface clinker–substrate.

In both samples, the SEM-EDS analysis of the original clinker (Table 4) confirmed that the C_3S phase and the liquid were the principal phases existing in the clinker.

The EDS microanalysis of the liquid phase nearest to the reaction zone (Table 4, zone 1), were very similar to the composition of the liquid phase of the original clinker for both substrates. Enrichments in ZrO_2 contents were detected, especially in the 20M–80CZ/C substrate, due to the presence of ZrO_2 small grains in the original substrate.

The thickness of the interaction zone (zone 2) in the 20M–80CZ/D substrate (Fig. 12b) was ~10 μm. This zone was constituted by small amount of liquid phase, sintered $CaZrO_3$ grains and a small amount of stable liquid phase trapped in triple points. The composition of this liquid phase is also shown in Table 4. As it can be observed, the composition of this phase was close to that of the liquid in zone 1 and only a little amount of ZrO_2 was detected. Small amounts of iron oxide, alumina, silica and magnesium oxide were detected in solid solutions in calcium zirconate grains.

In Fig. 14 an EDS mapping of Mg, Ca and Zr elements in the interaction zone of the 20M–80CZ/D sample is shown. Fig. 15 shows a complementary compositional profile (10 μm × 60 μm) in a perpendicular direction to the interaction zone. The compositional profile and the EDS mapping reveal small amounts of MgO remaining in the interaction zone. No significant differences in the content of Ca and Zr elements were observed by EDS mapping. However, the concentration profile evidences an increase in the CaO content as well as small amounts of Al_2O_3 and Fe_2O_3 in the interaction zone. These data can be related to the presence of a liquid phase (Table 4) located at the grain boundaries between the calcium zirconate grains, as described before. These results evidence the formation of a calcium zirconate layer at the interaction zone.

In the 20M–80CZ/C substrate (Fig. 13b) there was not evidence of any reaction zone formation. In fact, in the region closer to the clinker, only two or three layers of rounded $CaZrO_3$ grains and very small quantities of a liquid phase, compared with the previous sample, were observed; no MgO grains were observed. The composition of the liquid phase (Table 4) shows a considerable quantity of ZrO_2 due to the dissolution of ZrO_2 present in the substrate into the liquid. Silicon oxide and calcium oxide content in the liquid were also higher than those observed in the original clinker, since iron oxide and alumina diffused to the substrate and enter in solid solution in calcium zirconate grains. Small amounts of silica and magnesium oxide were also detected in solid solution in calcium zirconate grains.

In both samples, below the interaction zone, the substrates keep their initial microstructure, and only the presence of a small quantity of liquid phase diffused from the zone 2, through grain boundaries and porosity, was observed specially in 20M–80CZ/D sample. The preferential diffusion of Fe_2O_3 caused the coloration of the substrates, specially marked in 20M–80CZ/D due to relatively higher liquid content of this substrate.

These results together with the composition of the liquid phase determined by EDS (Table 2) in different fields, reveal, in good agreement with phase equilibrium studies, that MgO is less soluble in the liquid phase than $CaZrO_3$. The ZrO_2 content in the liquid phase varied from 6.5 to 11.5 wt.%, which is in good agreement with the solubility limit of zirconium oxide in silicate melts, while MgO content in liquid phase varied between 2.0 and 5.0 wt.%, values clearly less than the previous ones.

3.3. Clinker–substrates corrosion process

From the established isothermal section at 1500 °C, the corrosion behavior of both substrates can be described in terms of the connection line between the clinker and the substrate compositions (Fig. 5), which passes through the ($C_3S + L$), ($C_3S + CaZrO_3 + L$) and ($C_3S + CaZrO_3 + MgO + L$) stability compatibility fields.

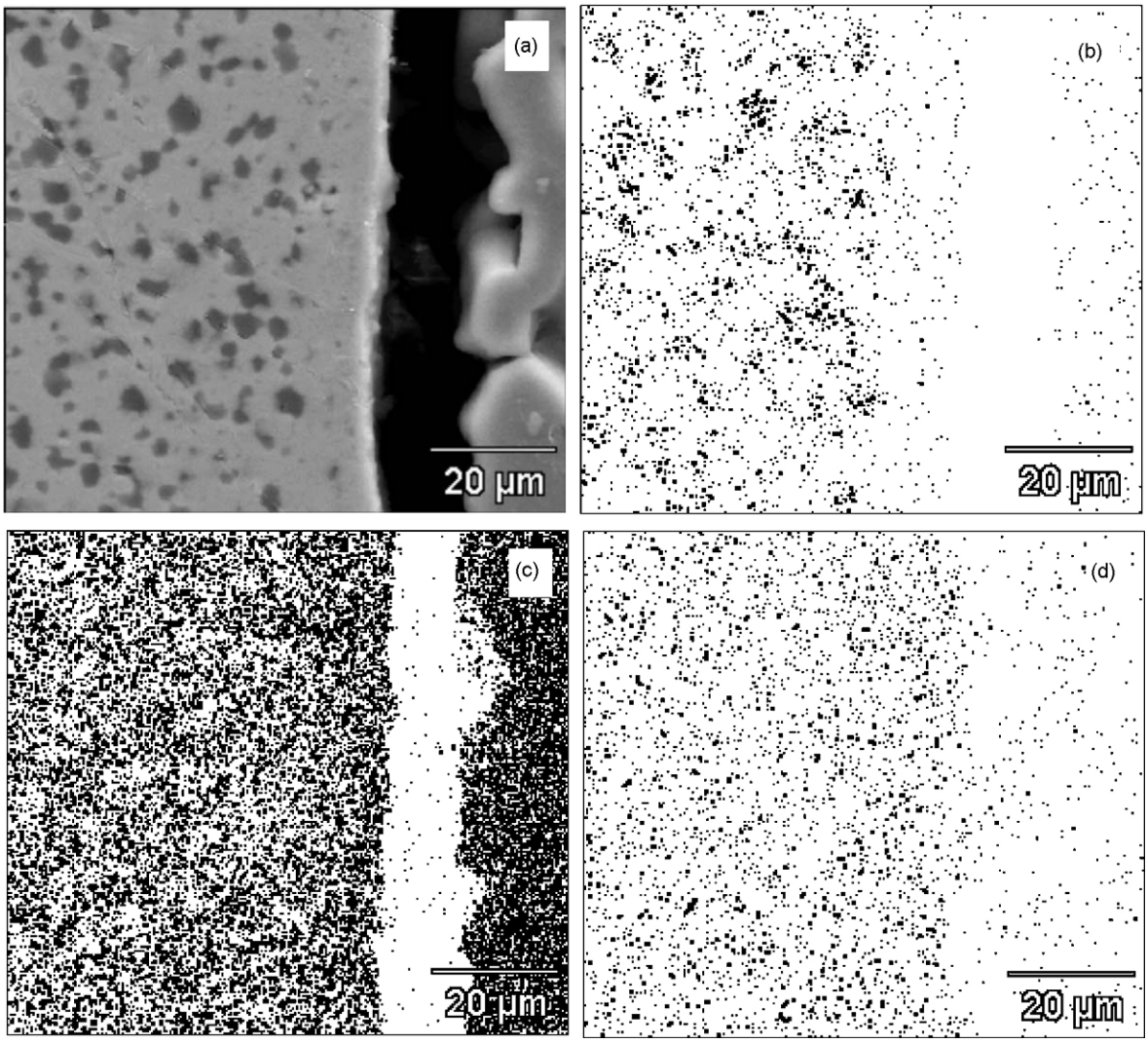

Fig. 14. Sample Clinker–20M–80CZ/D substrate treated at 1500 °C/3 h. SEM image of the interaction zone (a) EDS mappings of Mg (b), Ca (c) and Zr (d) elements.

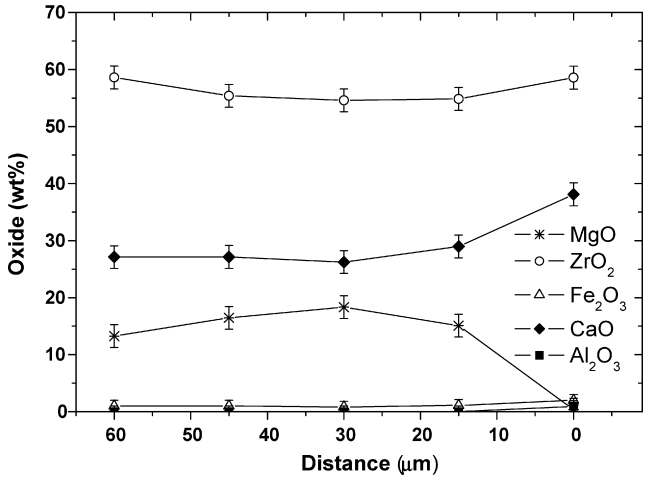

Fig. 15. Compositional profiles (10 μm × 60 μm) of the Clinker–20M–80CZ/D substrate treated at 1500 °C/3 h. Substrate surface has been taken as reference.

At the beginning of the corrosion process (1500 °C/1 min), the liquid phase of clinker penetrates into substrates through the open porosity and grain boundaries. Then, according to the predictions of the isothermal section, in a very narrow zone on the substrate surfaces, MgO is fully dissolved while $CaZrO_3$ is only partially dissolved (Figs. 10 and 11). At this point, the interaction between clinker and substrates lies on the line which separates the ($C_3S + L$) and ($C_3S + CaZrO_3 + L$) fields (Fig. 5).

Corrosion continues with the dissolution of more MgO and $CaZrO_3$ until the liquid is saturated in MgO, CaO and ZrO_2. At this point, the liquid composition is in equilibrium with C_3S, MgO and $CaZrO_3$ and consequently the attack process is ending. The composition at the interface reaches the (MgO $+C_3S + CaZrO_3 + L$) field.

The dissolution of MgO in a very narrow area of substrates leads to the formation and sintering of a layer of $CaZrO_3$ layer, with liquid phase in triple points. Under this layer, the substrates are constituted by $CaZrO_3$, MgO and a small amount of liquid phase.

In spite of these similarities, some differences were observed in the corrosion behavior between both substrates. These

differences are strongly related not only with their microstructural features, but also with the presence of free-ZrO_2 in the 20M–80CZ/C substrate. The fine grain size of 20M–80CZ/D substrate facilities the penetration of liquid phase and the dissolution processes producing a faster corrosion process and a larger size of the reaction zone. A larger colored region was also observed into this substrate, which is justified by the mentioned microstructural characteristics.

The bigger grain size of both MgO and $CaZrO_3$ and the presence of free ZrO_2 in the 20M–80CZ/C substrate leads to a slower dissolution process. The presence of Zr^{4+} in the liquid phase increases its viscosity and hinders the diffusion mechanism, improving the corrosion behavior of this material.

In addition, it is important to remark, that the attack does not cause the formation of cracks inside the substrate in any step of the process. However, a longitudinal crack is present in the samples after thermal treatments. These cracks are produced by the differences in the thermal expansion coefficients during the sample cooling. At the beginning of the corrosion process, the crack is located on the clinker–substrate interface, so that, a layer of clinker remains adhered to the surface of the substrates. In contrast, at the end of the corrosion process, the crack is located between the clinker and the substrate. This different behavior is related to the microstructure developed in the clinker–substrate interface during the attack. At the beginning of the corrosion process there is a continuos region where $CaZrO_3$, C_3S and a continuous liquid phase coexist at the interface, so that the crack produced by cooling appears in the clinker. At the end of the attack, the formation of the $CaZrO_3$ sintered layer on top of the substrates interrupts the continuity of the interface and propitiates the appearance of the crack along the clinker–substrate interface during cooling. Consequently, it is very important that at high temperature, liquid and solid phases coexist in equilibrium in a continuous region so that no cracks will appear. This mechanism is essential to prevent the corrosion of the refractory brick under work conditions[6,7] since the clinker layer will be formed whenever microstructural continuity exists at the interface.

From results previously reported by the present authors[8] and these herein reported, valuables practical implications can be obtained. The ratio $CaZrO_3$/MgO in the matrix can be selected to form a dense layer of $CaZrO_3 + L$ or $MgO + L$ to prevent the attack. Matrix formulation must consider the limits defined by the isothermal section studied. At the interface, low $CaZrO_3$/MgO ratios produce MgO layer while high $CaZrO_3$/MgO ratios produce $CaZrO_3$ layer.

The sintered layer of $CaZrO_3$ formed on the rich-$CaZrO_3$ substrate is thicker than the sintered MgO layer formed on the rich-MgO substrate, and moreover the dissolution of $CaZrO_3$ in "fresh clinker" is higher than MgO. This means that the formation of an MgO layer is more advantageous to prevent attack to the refractory, from a practical point of view. Calcium zirconate must be added to refractory matrices to saturate liquid phase in zirconium oxide to increase its viscosity and hence hinder its diffusion thorough the grain boundary and porosity.

4. Conclusions

The isothermal section Clinker–MgO–$CaZrO_3$ at 1500 °C has been experimentally established. In this section, the $CaZrO_3$/MgO ratio (1.5 ± 0.5), which defines the precipitation of $CaZrO_3$ or MgO as a secondary crystalline phase, has been deduced.

The results evidence that calcium zirconate is more soluble than MgO in clinker at 1500 °C and that the microstructural features of the substrates determine the corrosion rate. The corrosion process of refractory matrices (20% MgO–80% $CaZrO_3$) by clinker yields a $CaZrO_3$ sintered layer at the interaction zone.

An important practical implication has been deduced; the $CaZrO_3$/MgO ratio in the refractory matrix determines the formation of a dense layer of $CaZrO_3$ or MgO at the clinker interface.

Acknowledgements

The authors wish to acknowledge the financial support of the CICYT, Spain. Projects MAT 2004-04923-C02-01 and MAT 2007-65857.

References

1. Bartha, P. and Klischat, H. J., Present state of the refractory lining for cement kilns. *CN-Refractories*, 1999, **6**(3), 31–38.
2. Bray, D. J., Toxicity of chromium compounds formed in refractories. *Ceram. Bull.*, 1985, **64**(7), 1012–1016.
3. Driscoll, M. O., Price temper steel market promise. *Ind. Miner.*, 1994, **324**, 35–49.
4. Serena, S., Sainz, M. A., De Aza, S. and Caballero, A., Experimental determination and thermodynamic calculation of the ZrO_2–CaO–MgO phase equilibria diagram. Isothermal sections at 1600 °C, 1700 °C and 1750 °C. *J. Am. Ceram. Soc.*, 2004, **87**(12), 2268–2274.
5. Serena, S., Sainz, M. A., De Aza, S. and Caballero, A., Thermodynamic assesment of the system ZrO_2–CaO–MgO using new experimental results. Calculation of the isopletal section dolomia-zircona. *J. Eur. Ceram. Soc.*, 2005, **25**(5), 681–693.
6. Kozuka, H., Kaita, Y., Tuchiya, Y., Honda, T. and Ohta, S., New kind of chrome-free (MgO–CaO–ZrO_2) bricks for burning zone of rotary cement kiln. In: *Unitecr, vol. 93*, Sao Paulo, Brasil, 1993, pp. 1027–1037.
7. Kozuka, H., Kaita, Y., Tuchiya, Y., Honda, T. and Ohta, S., Further improvements of MgO-CaO-ZrO_2 bricks for burning zone of rotary cement kiln. In: *Unitecr, vol. 95*, Kyoto, Japan, 1995, pp. 256–263.
8. Serena, S., Sainz, M. A. and Caballero, A., Corrosion behavior of MgO/$CaZrO_3$ refractory matrix by clinker. *J. Eur. Ceram. Soc.*, 2004, **24**(8), 2399–2406.
9. Rodríguez-Galicia, J. L., de Aza, A. H., Rendoĭn-Angeles, J. C. and Pena, P., The mechanism of corrosion of MgO–$CaZrO_3$–calcium silicate materials by cement clinker. *J. Eur. Ceram. Soc.*, 2007, **27**(1), 79–89.
10. Park, J. H., Formation of $CaZrO_3$ at the interface between CaO–SiO_2–MgO–CaF_2(–ZrO_2) slags and magnesia refractories: computational and experimental study. *Calphad*, 2007, **31**(2), 149–154.
11. Taylor, J. R. and Dinsdale, D. A. T., Thermodynamic and phase diagram data for the CaO–SiO_2 system. *Calphad*, 1990, **14**(1), 71–88.
12. Mao, H., Hillert, M., Selleby, M. and Sundman, B., Thermodynamic of the CaO–Al_2O_3–SiO_2 system. *J. Am. Ceram. Soc.*, 2008, **89**(1), 298–308.
13. Lea, F. M. and Parker, T. W., Investigations on a portion of the quaternary system CaO–Al_2O_3–SiO_2–Fe_2O_3: the quaternary system CaO–2CaO·SiO_2–5CaO·3Al_2O_3–4CaO·Al_2O_3·Fe_2O_3. *Trans. Roy. Soc. (Lond.) Ser. A*, 1934, **234A**(731), 16.

14. Jak, E., Thermodynamic modelling of the system Al_2O_3–SiO_2–CaO–FeO–Fe_2O_3 to predict the flux requirements for coal ash slag. *Fuel Energy Abst.*, 1998, **39**(3), 231–232.
15. Fabrichnaya, O. B. and Nerat, I., Thermodynamic properties of liquid phase in the $CaO{\cdot}SiO_2$–$CaO{\cdot}Al_2O_3{\cdot}2SiO_2$–$2CaO{\cdot}Al_2O_3{\cdot}SiO_2$ system. *J. Eur. Ceram. Soc.*, 2000, **20**(4), 505–515.
16. Vázquez, B. A., Caballero, A. and Pena, P., Primary crystallization volume of alumina in the quaternary system Al_2O_3–CaO–SiO_2–MgO. *Bol. Soc. Esp. Ceram y V.*, 2004, **43**(1), 16–18.
17. Vázquez, B. A., Caballero, A. and Pena, P., Quaternary system Al_2O_3–CaO–SiO_2–MgO. II. Study of the crystallization volume of $MgAl_2O_4$. *J. Am. Ceram. Soc.*, 2005, **88**(7), 1949–1957.
18. Serry, M. A. and Barbulescu, A., Thermal-equilibrium of magnesia-dolomite refractories within the system CaO–MgO–C_2S–C_4AF. *Trans. J. Br. Ceram. Soc.*, 1981, **80**(6), 196–201.
19. De Aza, A. H., Iglesias, J. E., Pena, P. and De Aza, S., The ternary system Al_2O_3–MgO–CaO. Part II. Phase relationships in the subsystem Al_2O_3–$MgAl_2O_4$–$CaAl_4O_7$. *J. Am. Ceram. Soc.*, 2000, **83**(4), 919–927.
20. Pena, P., Vázquez, B., Caballero, A. and De Aza, S., Quaternary phase equilibrium diagrams. Representation and interpretation methods. *Bol. Soc. Esp. Ceram. y V.*, 2005, **44**(2), 113–122.
21. De Aza, S., Richmond, C. and White, J., Compatibility relationships of periclase in the system CaO–MgO–ZrO_2–SiO_2. *Trans. J. Br. Ceram. Soc.*, 1974, **73**(4), 109–116.
22. Taylor, H. F. W., *Cement Chemistry* (*2nd ed.*). Thomas Telford, London, 1997.
23. Matsumoto, K., Sawamoto, T. and Koide, S. The system CaO–SiO_2–ZrO_2. *Asahi Garasu Kenkyu Hokoku*, 1954, **4**(2), 8–10 [Phase Diagrams for Ceramists. Levin, E.M., Robbins, C.R., McMurdie, H.F., Editor Reser, M.K. Ed. by Am. Ceram. Soc., Columbus, Ohio, 1964].
24. Rodriĭguez, J. L., Rodriĭguez, M. A., De Aza, S. and Pena, P., Reaction sintering of zircon-dolomite mixtures. *J. Eur. Ceram. Soc.*, 2001, **21**(3), 343–354.
25. Serena, S., Caballero, A., Sainz, M. A., Convert, P., Campo, J. and Turrillas, X., Neutron thermodiffactometry study of calcium zirconate/magnesium oxide formation in the ZrO_2–CaO–MgO system. *J. Am. Ceram. Soc.*, 2004, **87**(9), 1706–1713.